Supplementary information

$UN@C_{82}$: A U≡N Triple Bond Captured inside Fullerene Cages

Qingyu Meng,[1,5] Laura Abella,[2,5] Yang-Rong Yao,[3] Dumitru-Claudiu Sergentu,[2] Wei Yang,[1] Xinye Liu,[1] Jiaxin Zhuang,[1] Luis Echegoyen,[4] Jochen Autschbach[1,*] and Ning Chen[1,*]

[1] College of Chemistry, Chemical Engineering and Materials Science, and State Key Laboratory of Radiation Medicine and Protection, Soochow University, Suzhou, Jiangsu 215123, P. R. China.

[2] Department of Chemistry, University at Buffalo, State University of New York. Natural Sciences Complex. Buffalo, NY 14260-3000, United States.

[3] Department of Materials Science and Engineering, University of Science and Technology of China, Hefei 230026, China.

[4] Department of Chemistry, University of Texas at El Paso, 500 W University Avenue, El Paso, Texas 79968, United States.

[5] These authors contributed equally: Qingyu Meng, Laura Abella.

* Correspondence authors: chenning@suda.edu.cn; jochena@buffalo.edu.

Supplementary Discussion: Synthesis and isolation of UN@C_s(6)-C_{82} and UN@C_2(5)-C_{82} 5

Supplementary Figures

Fig. 1. HPLC chromatogram of purified UN@C_s(6)-C_{82} and UN@C_2(5)-C_{82}. 6

Fig. 2. HPLC separation of UN@C_s(6)-C_{82} 7

Fig. 3 HPLC separation of UN@C_2(5)-C_{82} 8

Fig. 4. Ball and stick representation of disordered cage and U/N sites in UN@C_2(5)-C_{82} at 100 K. 9

Fig. 5. The interaction of the major U site (a) U1 and (b) U1A with the closest cage in UN@C_2(5)-C_{82} at 100 K 9

Fig. 6. Ball and stick representation of U sites and N sites in UN@C_s(6)-C_{82}. at 100 K 10

Fig. 7. ADF/PBE/TZP/D3 optimized UN@C_2(5)-C_{82} and UN@C_s(6)-C_{82} geometries (blue is N and light blue is U). 10

Fig. 8. Single-crystal X-ray structure of UN@C_s(6)-C_{82}·[Ni^{II}(OEP)] measured at 100 and 185 K. 11

Fig. 9. Molecular structure of UN@C_2(5)-C_{82} measured with single crystal X-ray diffraction at variable temperatures from 100 K to 273 K. 12

Fig. 10. ZORA/PBE/TZP/D3 optimized UN@C_2(5)-C_{82} spin-doublet geometries with different orientation of the UN cluster inside the C_2-C_{82} cage. 12

Fig. 11. ZORA/PBE/TZP/D3 optimized UN@C_s(6)-C_{82} spin-doublet geometries with different orientation of the UN cluster inside the C_s-C_{82} cage. 12

Fig. 12. Partial molecular orbital (MO) diagram obtained with ZORA/PBE/TZP/D3 for the ground spin-doublet state of UN@C_2(5)-C_{82} and UN@C_s(6)-C_{82}. 13

Fig. 13. NLMO isosurfaces (±0.03 a.u.) of the carbon cage and atomic orbital %-compositions obtained from a natural bond orbital analysis of the ZORA/DFT/PBE/NBO6.0 doublet state obtained for UN@C_2(5)-C_{82}. 13

Fig. 14. NLMO isosurfaces (±0.03 a.u.) of the carbon cage and atomic orbital %-

compositions obtained from a natural bond orbital analysis of the ZORA/DFT/PBE/NBO6.0 doublet state obtained for UN@C_s(6)-C_{82}..... 14

Fig. 15. Molecular orbital (MO) diagram obtained with ZORA/PBE/TZP/D3 for the ground spin-quartet state of UN and spin-doublet state of UN^{2+}..... 15

Fig. 16. Isosurface (±0.01 a.u.) of the spin density (SD) distribution for the spin-quartet state UN and spin-doublet state of UN^{2+}. 15

Fig. 17. NLMO isosurfaces (±0.03 a.u.) and atomic orbital %-compositions obtained from a natural bond orbital analysis of the ZORA/DFT/PBE/NBO6.0 doublet state obtained for UN^{2+}. 15

Fig. 18. NLMO isosurfaces (±0.03 a.u.) and atomic orbital %-compositions obtained from a natural bond orbital analysis of the ZORA/DFT/PBE/NBO6.0 quartet state obtained for UN. 16

Fig. 19. XAMS-CASPT2(-SO) Potential Energy Surface (PES) scans along the internuclear distance of UN (left) and UN^{2+} (right)..... 16

Fig. 20. UV−vis−NIR spectra of UN@C_s(6)-C_{82} and UN@C_2(5)-C_{82} 17

Fig. 21. Low energy Raman spectra of UN@C_s(6)-C_{82} and UN@C_2(5)-C_{82}. Computed low energy Raman spectra for the spin-doublet ground state geometries of UN@C_2(5)-C_{82} and UN@C_s(6)-C_{82}..... 17

Fig. 22. Vibrational normal modes of UN@C_2(5)-C_{82} assigned to the major peaks in the low-energy Raman spectra..... 18

Fig. 23. Vibrational normal modes of UN@C_s(6)-C_{82} assigned to the major peaks in the low-energy Raman spectra..... 18

Fig. 24. Single-crystal X-ray structure of UN@C_s(6)-C_{82}·[Ni^{II}(OEP)] measured at 100 to 273 K..... 18

Supplementary Tables

Table 1. The distance between U1 and C_{cage} in UN@C_2(5)-C_{82} at 100 K 19

Table 2. The distance between U1 and C_{cage} in UN@C_s(6)-C_{82} at 100 K..... 19

Table 3. Adiabatic spin-state relative energies (ΔE, kcal·mol^{-1}), U Mulliken Spin Populations (MSP) and structural parameters (distances in Å) for UN@C_{82}..... 19

Table 4. Metal site occupancy in UN@C_s(6)-C_{82} as a function of temperatures. 20

Table 5. Metal site occupancy in UN@C_2(5)-C_{82} as a function of temperatures. 20

Table 6. Crystal data of UN@C_s(6)-C_{82} 21

Table 7. Crystal data of UN@C_2(5)-C_{82} 22

Table 8. Adiabatic spin-state relative energies (ΔE, kcal·mol^{-1}) and U Mulliken Spin Populations (MSP) for UN@C_2(5)-C_{82} and UN@C_s(6)-C_{82} using different functionals: PBE, BP86, PBE0 and B3LYP 23

Table 9. Comparison of the calculated N-U distance (in Å) using different functionals: PBE, BP86, PBE0 and B3LYP, vs. the experimental value for UN@C_2(5)-C_{82} and UN@C_s(6)-C_{82}. 23

Table 10. Adiabatic spin-state relative energies (ΔE, kcal·mol^{-1}) and U Mulliken Spin Populations (MSP) for UN@C_2(5)-C_{82} and UN@C_s(6)-C_{82} using different software: ADF vs. G16. 23

Table 11. Comparison of the calculated N-U distance (in Å) using ADF vs. G16. The data are compared to the corresponding experimental value for UN@C_2(5)-C_{82} and UN@C_s(6)-C_{82}. 23

Table 12. Relative energies (in kcal·mol^{-1}) and structural parameters (distances in Å) of UN, obtained with ZORA/PBE/TZP/D3 for optimized UN@C_2(5)-C_{82} spin-doublet geometries with different orientation of the UN cluster inside the C_2-C_{82} cage 24

Table 13. Relative energies (in kcal·mol^{-1}) and structural parameters (distances in Å) of UN, obtained with ZORA/PBE/TZP/D3 for optimized UN@C_s(6)-C_{82} spin-doublet geometries with different orientation of the UN cluster inside the C_s(6)-C_{82} cage 24

Table 14. U-N distance in UN@C_s(6)-C_{82} as a function of temperatures. 24

xyz coordinates 25

Supplementary Discussion

High-performance liquid chromatography (HPLC) separation process of UN@C_s(6)-C_{82}. The first stage was performed on a Buckyprep-M column (25 mm × 250 mm, Cosmosil Nacalai Tesque) with toluene as mobile phase. After that, as shown in Figure S1, fraction from 29 to 35 min (marked in red) was re-injected into a Buckyprep column (10 mm × 250 mm, Cosmosil Nacalai Tesque) for the second stage separation using toluene as the eluent. The fraction marked in orange, which contained UN@C_s(6)-C_{82} was collected. The third stage of separation was conducted on a 5PBB column (10 mm × 250 mm, Cosmosil Nacalai Tesque) using toluene as the eluent. The fraction marked in blue. The fourth stage was conducted on a BP column (10 mm × 250 mm, Cosmosil Nacalai Tesque) with a recycle method using toluene as the eluent. The fraction marked in magenta, which contained UN@C_s(6)-C_{82} was collected and re-injected into the Buckyprep-M column (10 mm × 250 mm, Cosmosil Nacalai Tesque) in the fifth stage. The final pure sample was obtained through the sixth stage, the sixth stage was conducted on a BP column (10 mm × 250 mm, Cosmosil Nacalai Tesque) with a recycle method again, and the final pure sample was the green part.

High-performance liquid chromatography (HPLC) separation process of UN@C_2(5)-C_{82}. The first stage was performed on a Buckyprep-M column (25 mm × 250 mm, Cosmosil Nacalai Tesque) with toluene as mobile phase. After that, as shown in Figure S2, fraction from 29 to 35 min (marked in red) was re-injected into a Buckyprep column (10 mm × 250 mm, Cosmosil Nacalai Tesque) for the second stage separation using toluene as the eluent. The fraction marked in orange, which contained UN@C_2(5)-C_{82} was collected. The third stage of separation was conducted on a 5PBB column (10 mm × 250 mm, Cosmosil Nacalai Tesque) using toluene as the eluent. The fraction marked in blue. The fourth stage was conducted on a BP column (10 mm × 250 mm, Cosmosil Nacalai Tesque) with a recycle method using toluene as the eluent. The fraction marked in pink, which contained UN@C_2(5)-C_{82} was collected and re-injected into the 5PBB column (10 mm × 250 mm, Cosmosil Nacalai Tesque) in the fifth stage. The UN@C_2(5)-C_{82} pure sample was finally obtained.

In total 2.02 g of graphite powder and 1.58 g of U_3O_8 (molar ratio of C:U = 30:1) were packed in each rod. On average ca. 40 mg of crude fullerene mixture per rod was obtained and totally 800 carbon rods were vaporized in this work. After HPLC isolation and purification process, ca. 0.2 mg purified UN@C_s(6)-C_{82} and UN@C_2(5)-C_{82} were obtained.

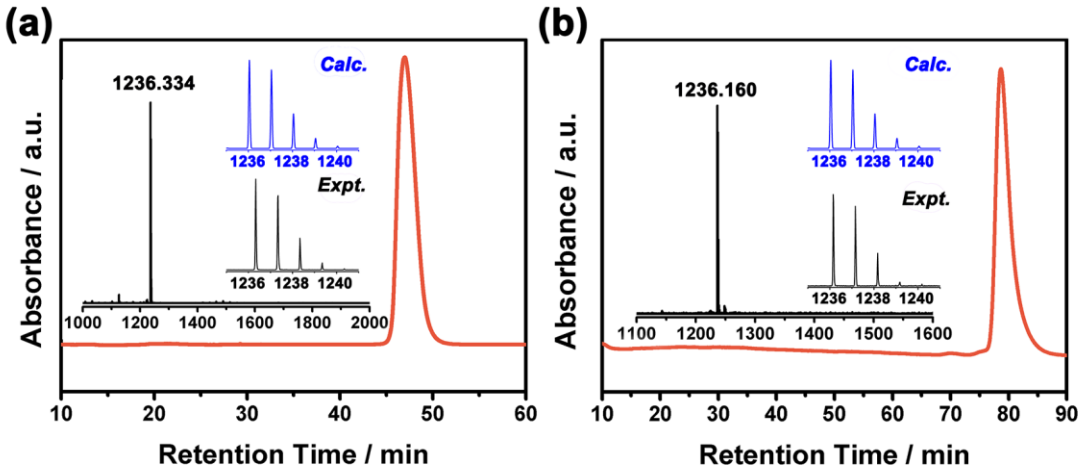

Supplementary Fig. 1 HPLC chromatogram of purified UN@C_s(6)-C_{82} and UN@C_2(5)-C_{82}. (a) UN@C_s(6)-C_{82} on a Buckyprep column and (b) UN@C_2(5)-C_{82} on a 5PBB column with toluene as the eluent. HPLC condition, λ = 310 nm; flow rate, 4 mL / min. The insets show the positive-ion mode MALDI-TOF mass spectra and expansions of the corresponding experimental isotopic distributions of the compound in comparison with their calculated ones.

Supplementary Figures

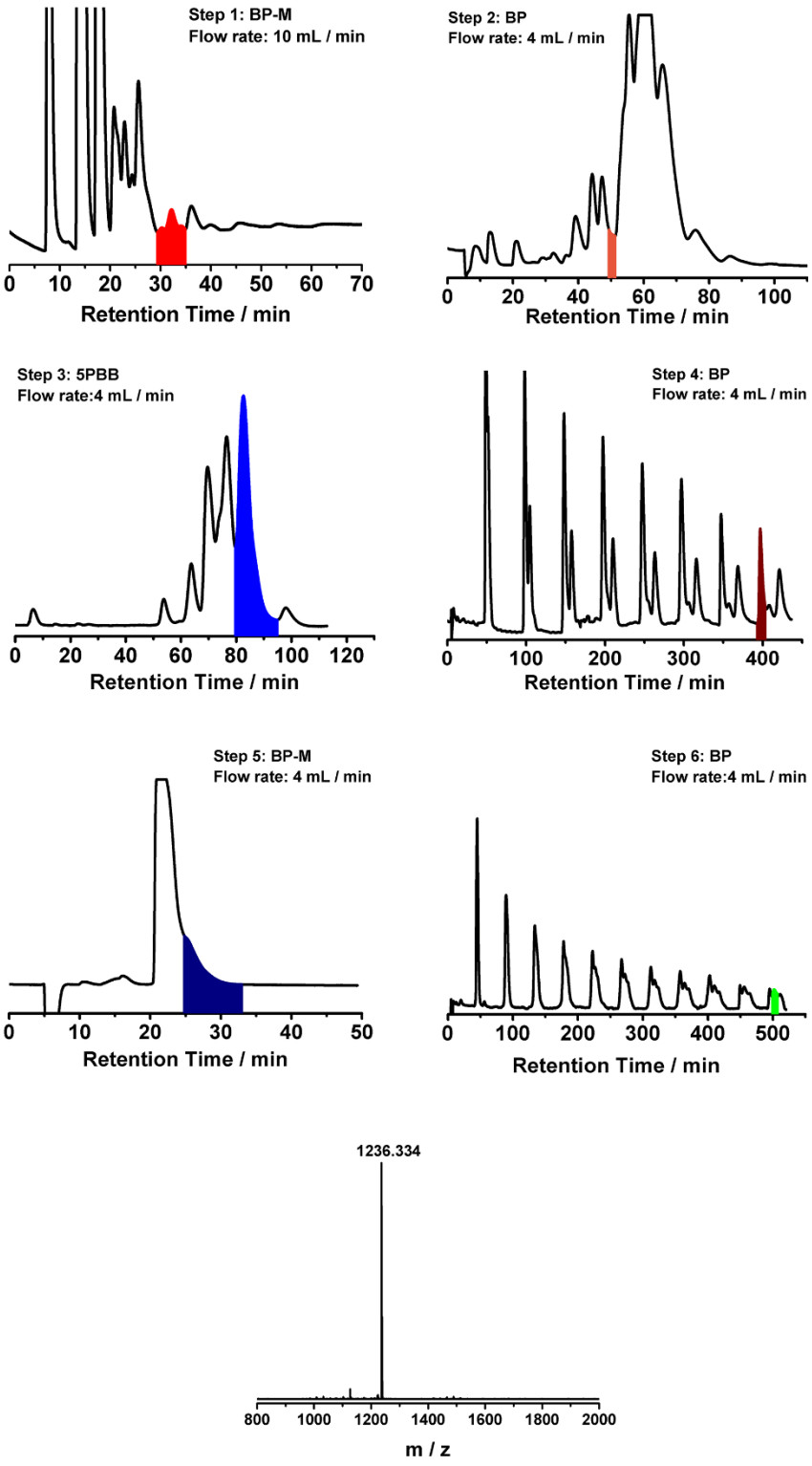

Supplementary Fig. 2 HPLC profiles showing the separation procedures of UN@C_s(6)-C_{82} and the pure sample's MALDI-TOF mass spectrum.

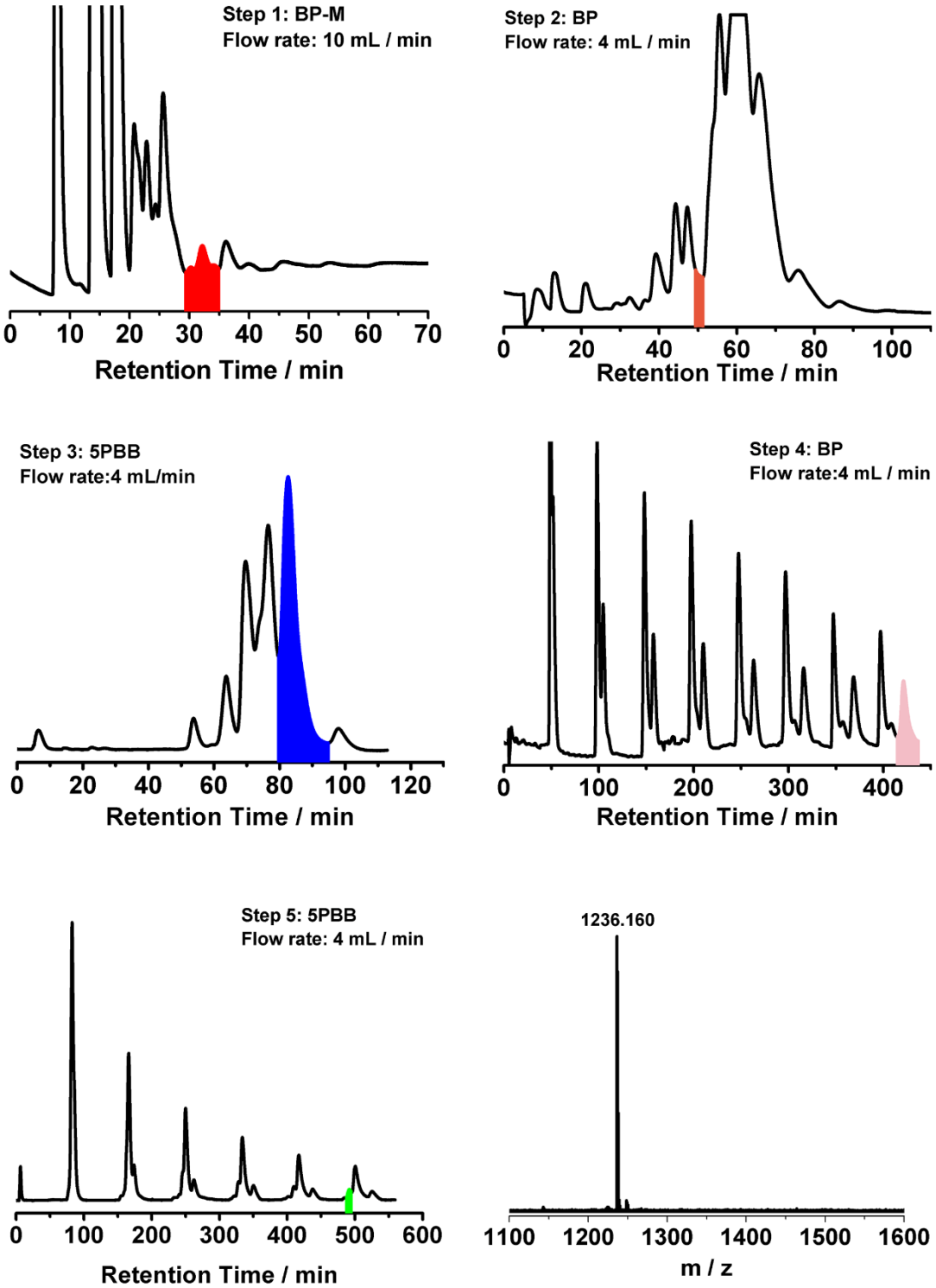

Supplementary Fig. 3. HPLC profiles showing the separation procedures of UN@C_2(5)-C_{82} and the pure sample's MALDI-TOF mass spectrum.

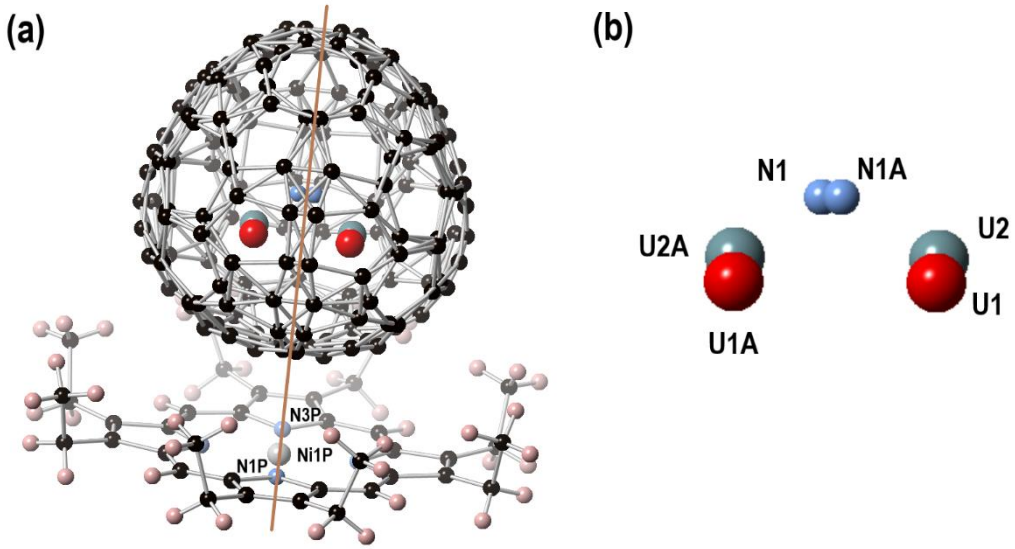

Supplementary Fig. 4. (a) Ball and stick representation of disordered cage and U/N sites in UN@C_2(5)-C_{82} at 100 K. (b) Drawing of all the U, N disordered sites, two disordered sites with fractional occupancies of 0.5 for N1 and N1A (which is generated from N1 atom by mirror plane of the crystal) atom, and four sites for U are presented, two disordered sites with fractional occupancies of 0.312 and 0.188 for U1 and U2, respectively. Another half of the U disordered sites (U1A, U2A, respectively) could be generated by mirror plane of the crystal which is vertically perpendicular to the paper plane.

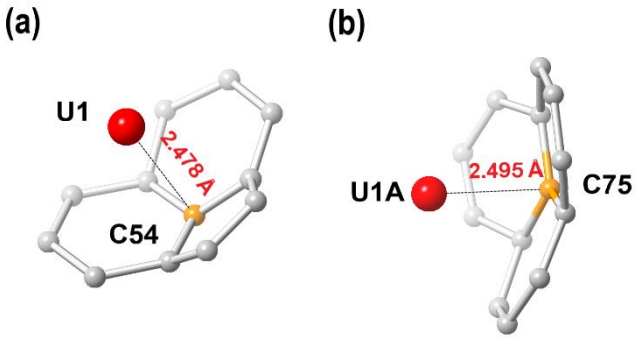

Supplementary Fig. 5. The interaction of the major U site (a) U1 and (b) U1A with the closest cage in UN@C_2(5)-C_{82} at 100 K.

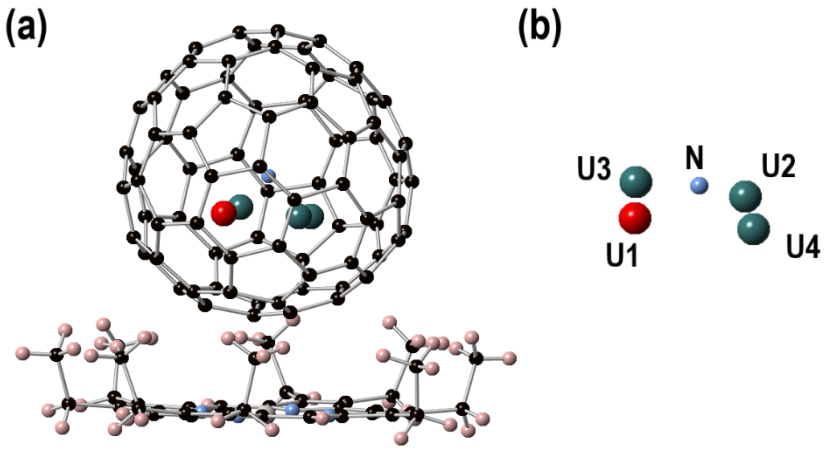

Supplementary Fig. 6. (a) Ball and stick representation of U sites and N sites in UN@C_s(6)-C_{82} at 100 K. (b) Drawing of all the U, N disordered sites, four disordered sites with fractional occupancies of 0.6442, 0.1903, 0.1087 and 0.0566 for U1, U2, U3 and U4 respectively.

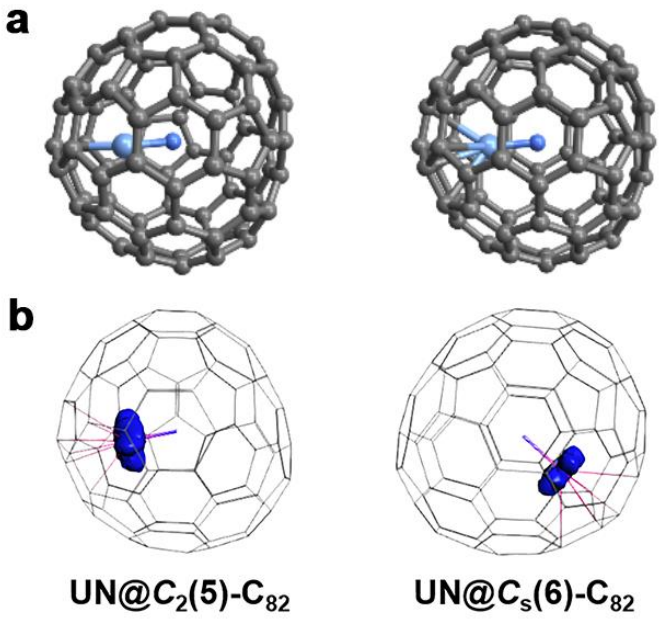

Supplementary Fig. 7. (a) ADF/PBE/TZP/D3 optimized UN@C_2(5)-C_{82} and UN@C_s(6)-C_{82} geometries (blue is N and light blue is U). (b) Isosurfaces (±0.01 au) of the calculated spin density for the optimized spin-doublet ground state structures of UN@C_2(5)-C_{82} (left) and UN@C_s(6)-C_{82} (right).

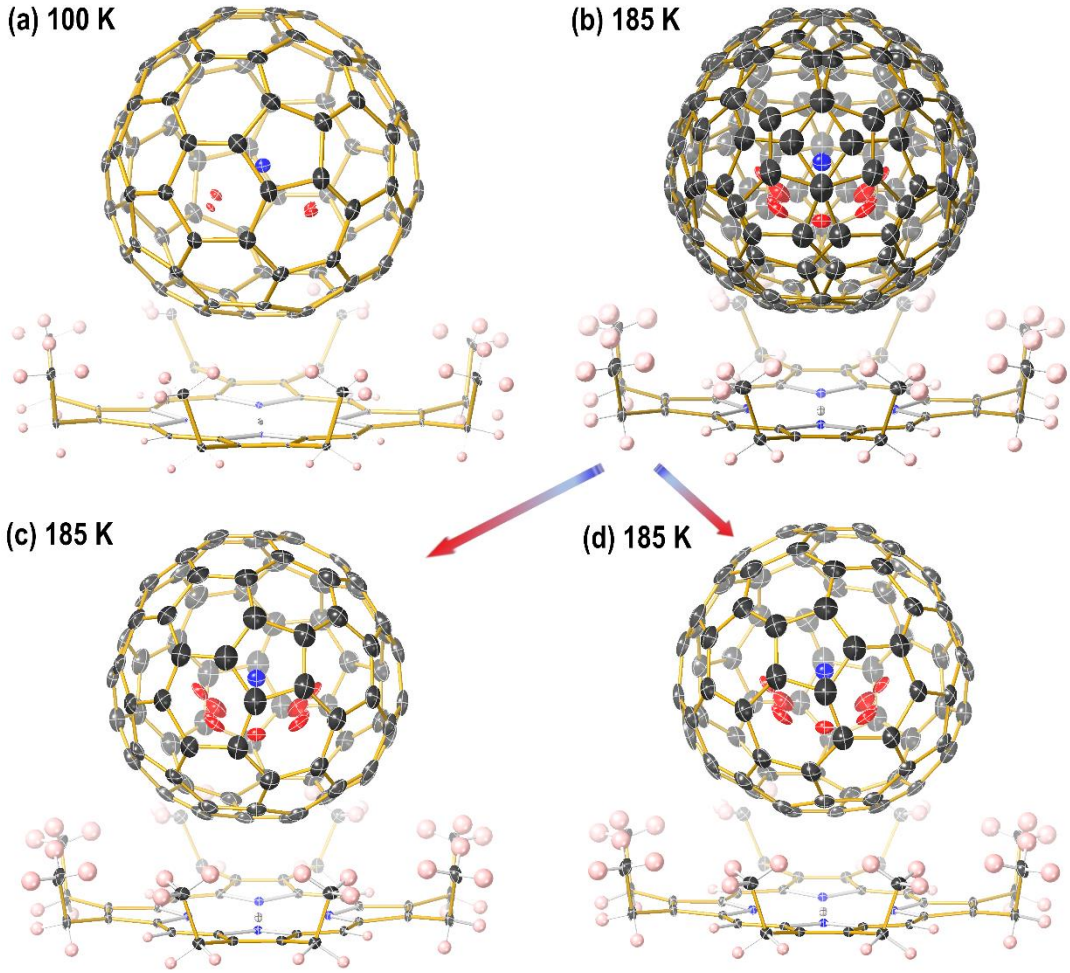

Supplementary Fig. 8. Single-crystal X-ray structure of UN@C_s(6)-C_{82}·[Ni^{II}(OEP)] measured at 100 and 185 K. Solvent molecules are omitted for clarity. The displacement parameters are shown at the 20% probability level. Color code: black for carbon, red for U, blue for N, pink for H, and grey for Ni. (a) The structure measured at 100 K is placed here for comparison. (b) The structure measured at 185 K shown with both orientations. (c, d) The two orientations of the structure measured at 185 K are split to view the structure in higher clarity.

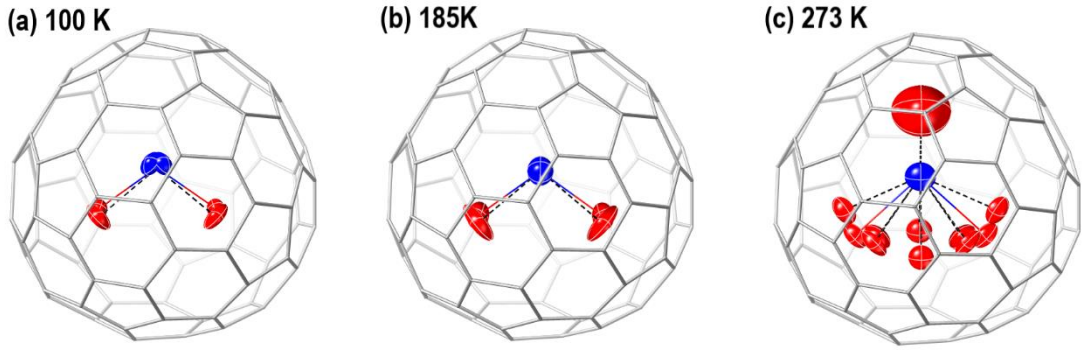

Supplementary Fig. 9. Molecular structure of UN@C_2(5)-C_{82} measured with single crystal X-ray diffraction at variable temperatures from 100 K to 273 K. The displacement parameters are shown at the 20 % probability level for the encapsulated UN cluster. The structures are drawn from the chosen specific direction of the crystal to compare the dynamics of the UN@C_2(5)-C_{82}. Color code: grey for C, blue for N, and red for U.

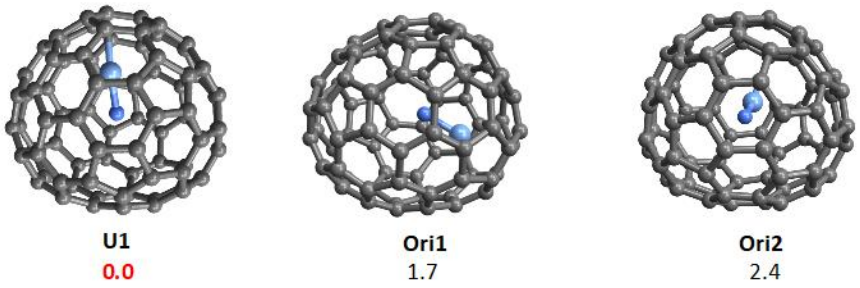

Supplementary Fig. 10. ZORA/PBE/TZP/D3 optimized UN@C_2(5)-C_{82} spin-doublet geometries with different orientation of the UN cluster inside the C_2-C_{82} cage. Relative energies in kcal·mol^{-1} are indicated below each orientation (Ori). U1 cage is the geometry optimized from the crystallographic data with the U position of U1.

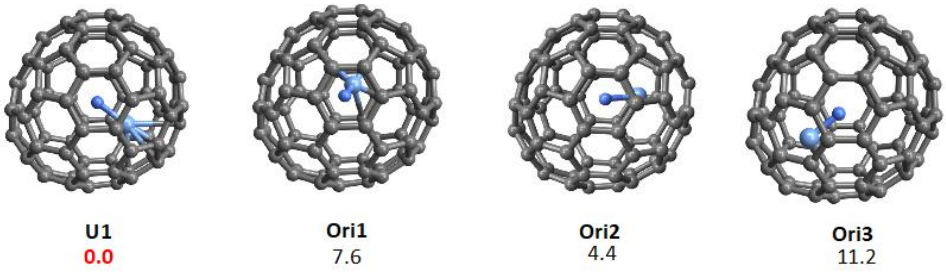

Supplementary Fig. 11. ZORA/PBE/TZP/D3 optimized UN@C_s(6)-C_{82} spin-doublet geometries with different orientation of the UN cluster inside the C_s-C_{82} cage. Relative energies in kcal·mol^{-1} are indicated below each orientation (Ori). U1 cage is the geometry optimized from the crystallographic data with the U position of U1.

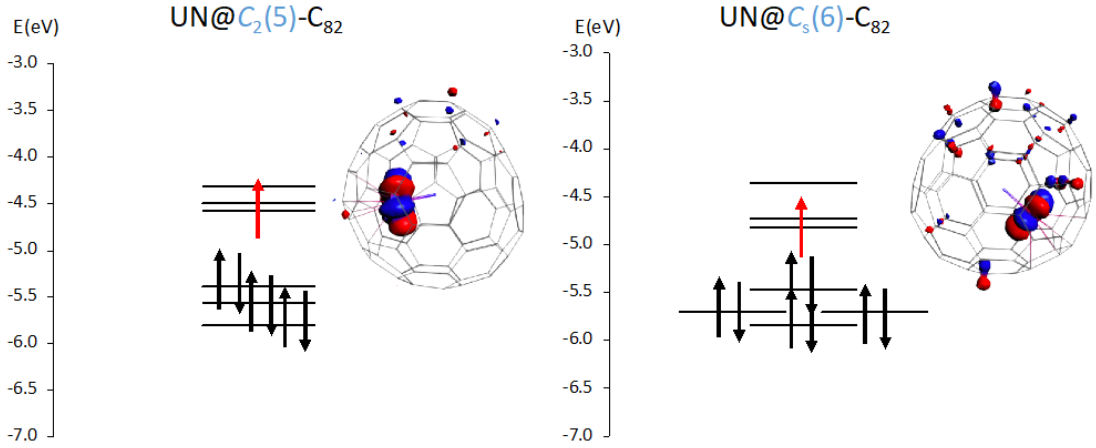

Supplementary Fig. 12. Partial molecular orbital (MO) diagram obtained with ZORA/PBE/TZP for the ground spin-doublet state of UN@C_2(5)-C_{82} (left) and UN@C_s(6)-C_{82} (right). The singly-occupied molecular orbital (for α-spin) is drawn in red and the associated MO isosurface (±0.04 a.u.) is shown on the side.

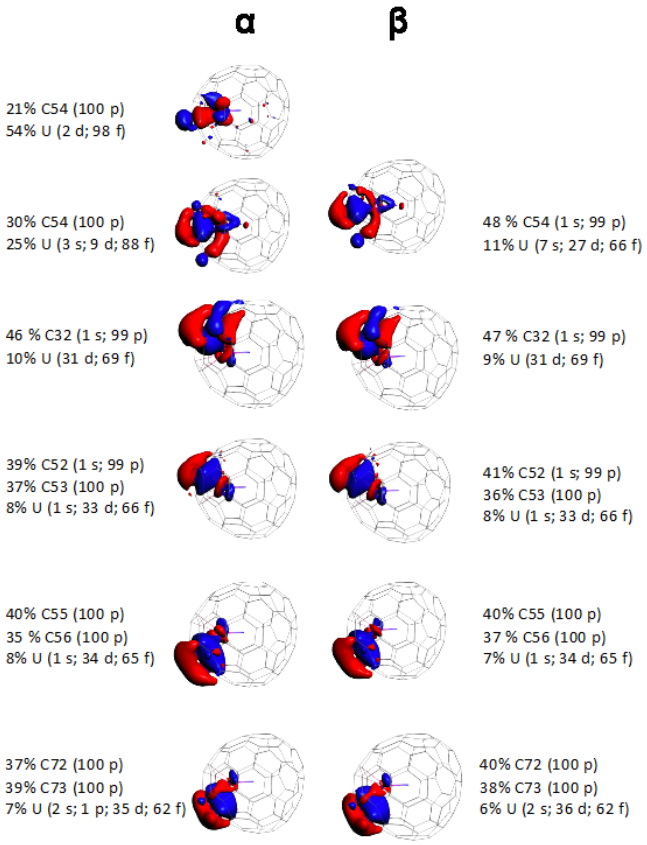

Supplementary Fig. 13. NLMO isosurfaces (±0.03 a.u.) of the carbon cage and atomic orbital %-compositions obtained from a natural bond orbital analysis of the ZORA/DFT/PBE doublet state obtained for UN@C_2(5)-C_{82}. Alpha (α)- and beta (β)-spins are plotted separately.

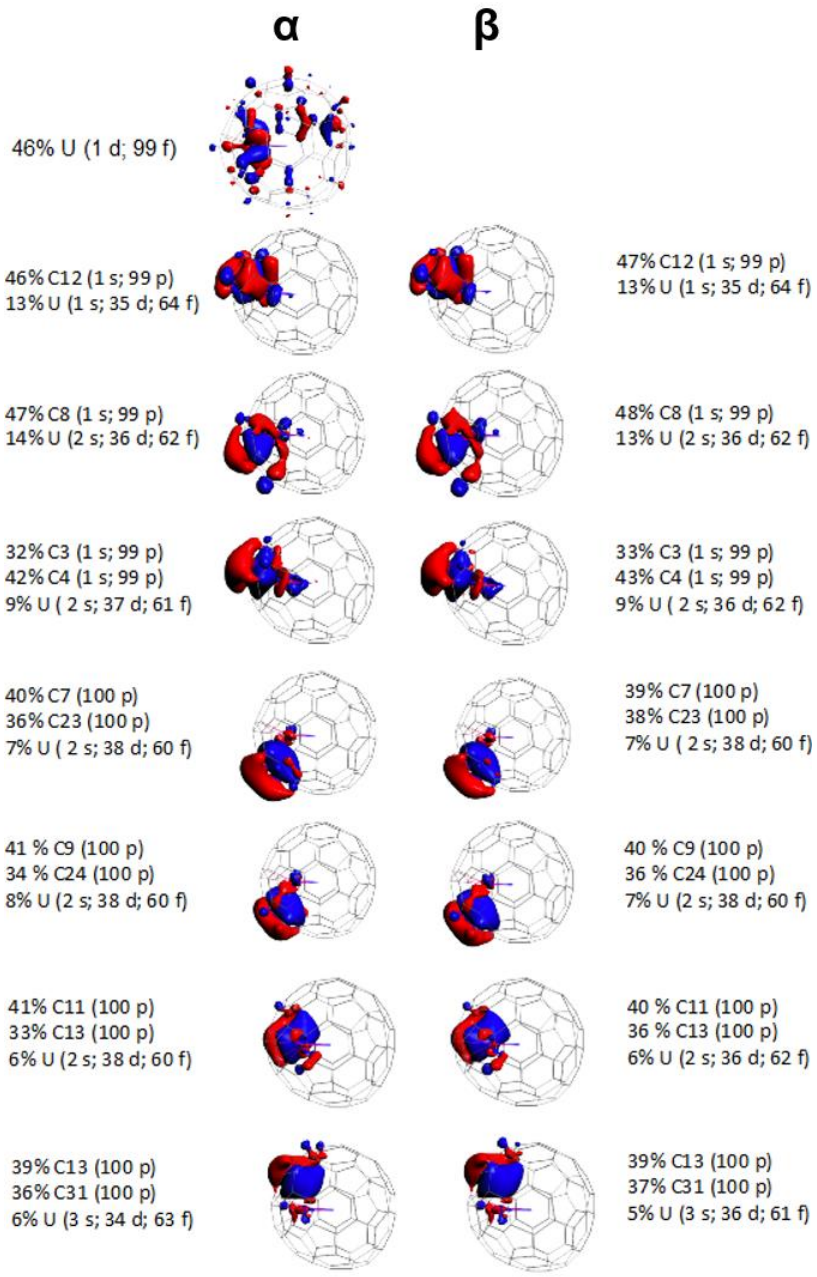

Supplementary Fig. 14. NLMO isosurfaces (±0.03 a.u.) of the carbon cage and atomic orbital %-compositions obtained from a natural bond orbital analysis of the ZORA/DFT/PBE doublet state obtained for UN@C_s(6)-C_{82}. Alpha (α)- and beta (β)-spins are plotted separately.

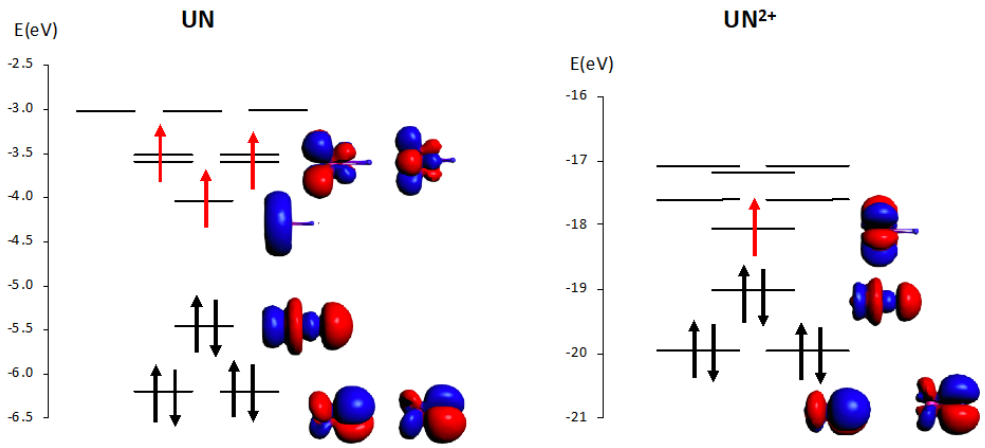

Supplementary Fig. 15. Molecular orbital (MO) diagram obtained with ZORA/PBE/TZP for the ground spin-quartet state of UN and spin-doublet state of UN^{2+}. The singly-occupied molecular orbitals (for α-spin) are drawn in red. MO isosurfaces (±0.04 a.u.) are shown on the side.

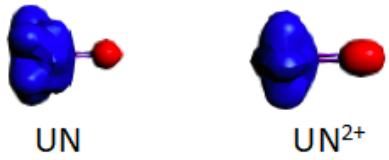

Supplementary Fig. 16. Isosurface (±0.01 a.u.) of the spin density (SD) distribution for the spin-quartet state UN and spin-doublet state of UN^{2+}.

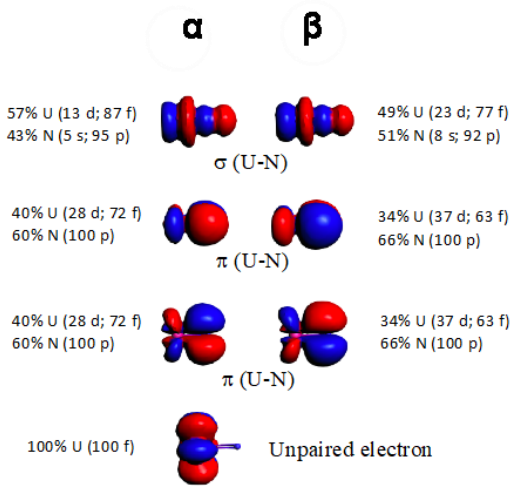

Supplementary Fig. 17. NLMO isosurfaces (±0.03 a.u.) and atomic orbital %-compositions obtained from a natural bond orbital analysis of the ZORA/DFT/PBE doublet state obtained for UN^{2+}. Alpha (α)- and beta (β)-spins are plotted separately.

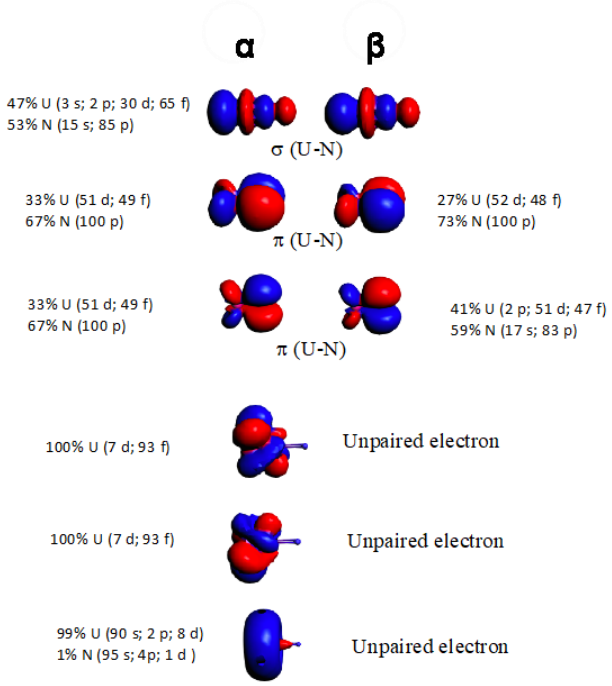

Supplementary Fig. 18. NLMO isosurfaces (±0.03 a.u.) and atomic orbital %-compositions obtained from a natural bond orbital analysis of the ZORA/DFT/PBE quartet state obtained for UN. Alpha (α)- and beta (β)-spins are plotted separately.

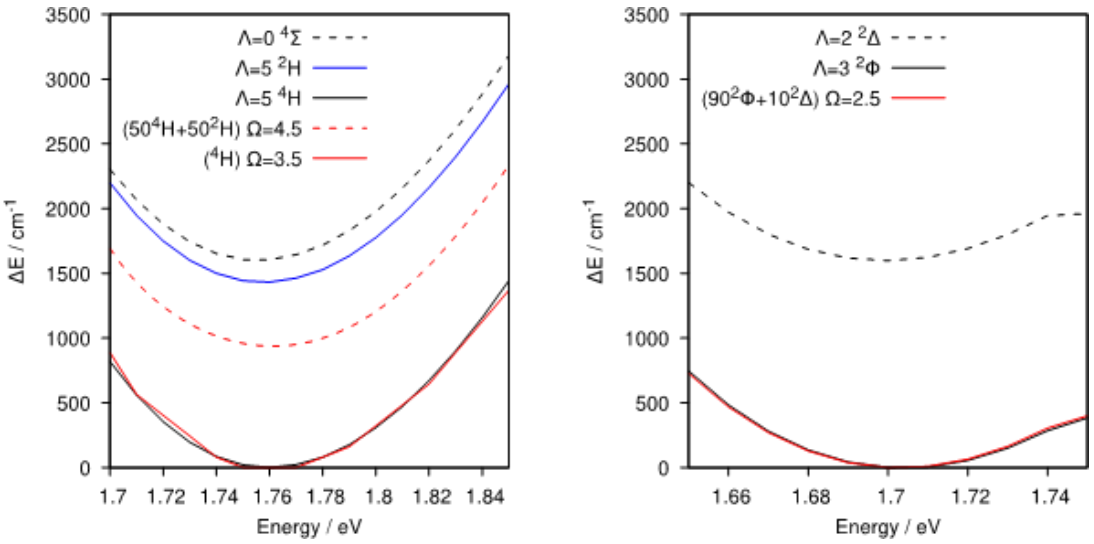

Supplementary Fig. 19. XAMS-CASPT2(-SO) Potential Energy Surface (PES) scans along the internuclear distance of UN (left) and UN^{2+} (right).

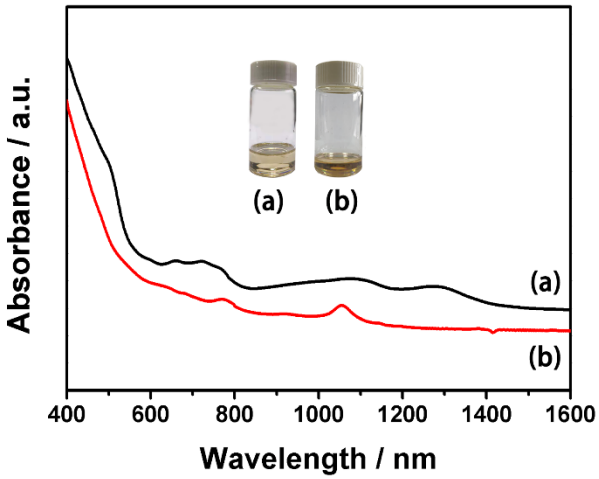

Supplementary Fig. 20. UV−vis−NIR spectra of (a) UN@C_s(6)-C_{82} and (b) UN@C_2(5)-C_{82} dissolved in CS_2. Insets: Photographs of the UN@C_{82}.

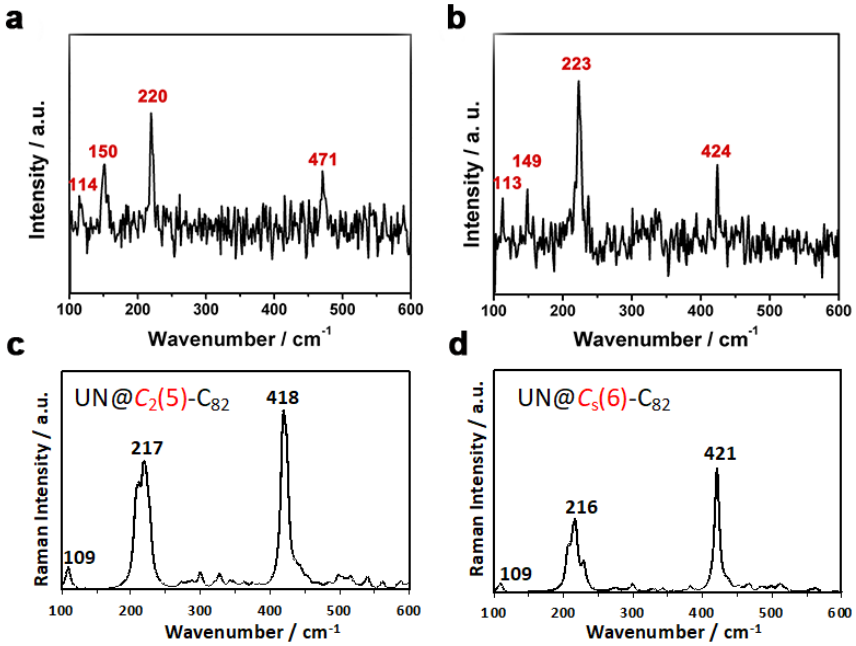

Supplementary Fig. 21. Low energy Raman spectra of (a) UN@C_s(6)-C_{82} and (b) UN@C_2(5)-C_{82} at 785 nm excitation. Computed low energy Raman spectra for the spin-doublet ground state geometries of (c) UN@C_2(5)-C_{82} and (d) UN@C_s(6)-C_{82}.

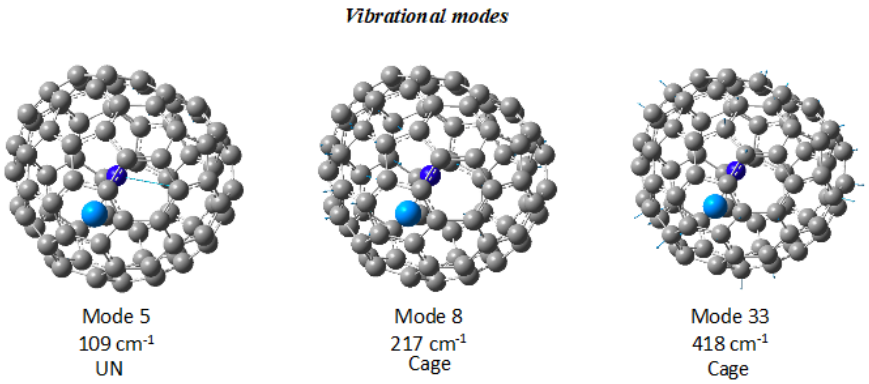

Supplementary Fig. 22. Vibrational normal modes of UN@C_2(5)-C_{82} assigned to the major peaks in the low-energy Raman spectra. For each mode, the wavenumber and arrows indicating the atoms that move are shown.

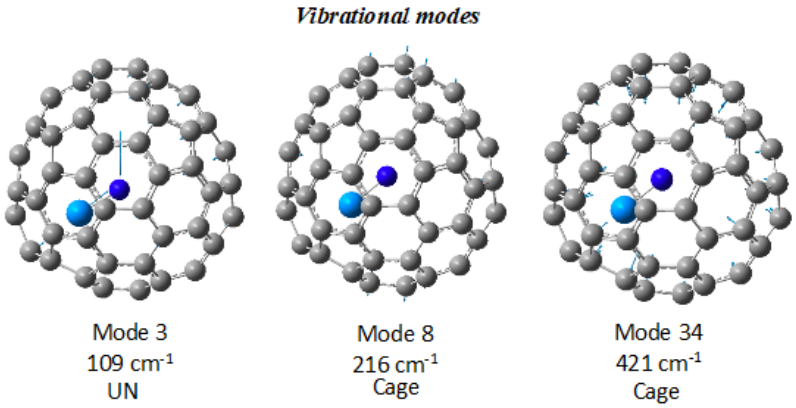

Supplementary Fig. 23. Vibrational normal modes of UN@C_s(6)-C_{82} assigned to the major peaks in the low-energy Raman spectra. For each mode, the wavenumber and arrows indicating the atoms that move are shown.

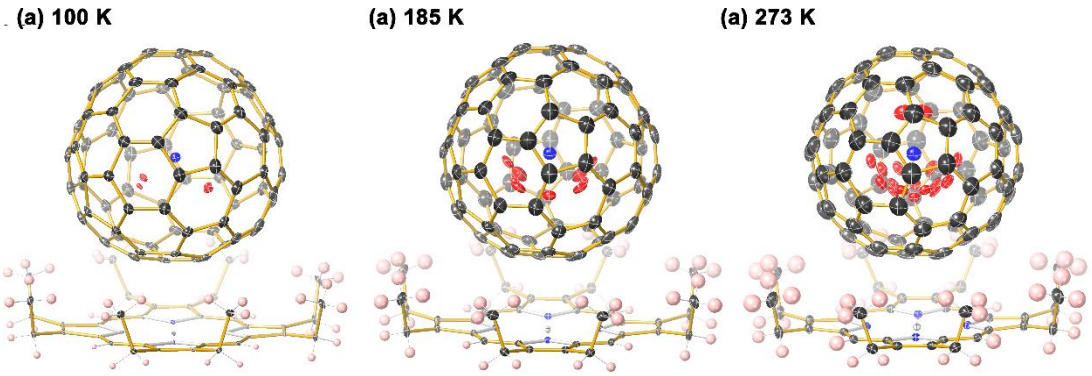

Supplementary Fig. 24. Single-crystal X-ray structure of UN@C_s(6)-C_{82}·[Ni^{II}(OEP)] measured at 100 to 273 K. Solvent molecules are omitted for clarity. The displacement parameters are shown at the 20% probability level. Color code: black for carbon, red for U, blue for N, pink for H, and grey for Ni.

Supplementary Tables

Supplementary Table 1. The distance between U1 and C_{cage} in UN@C_2(5)-C_{82} at 100 K.

Labelling	U-C54	U-C53	U-C72	U-C55
Length / Å	2.478	2.592	2.646	2.652

Supplementary Table 2. The distance between U1 and C_{cage} in UN@C_s(6)-C_{82} at 100 K.

Labelling	U-C1	U-C6	U-C10	U-C7
Length / Å	2.522	2.503	2.637	2.689

Supplementary Table 3. Adiabatic spin-state relative energies (ΔE, kcal·mol^{-1}), U Mulliken Spin Populations (MSP) and structural parameters (distances in Å) for UN@C_{82} isomers 5 and 6. Experimental values in parenthesis.

Isomer	Spin state	ΔE	MSP (U)	U-N	U-C1	U-C2	U-C3	U-C4
UN@ C_2(5)- C_{82}	Doublet	5.3	0.8	1.764 (1.760)	2.503 (2.478)	2.515	2.624	2.634
	Quartet	23.2	1.0	1.766	2.502	2.546	2.623	2.631
UN@ C_s(6)- C_{82}	Doublet	0.0	0.5	1.760 (1.760)	2.476 (2.503)	2.506 (2.522)	2.551	2.631
	Quartet	16.6	0.9	1.760	2.514	2.521	2.600	2.673

Supplementary Table 4. Metal site occupancy in UN@C_s(6)-C_{82} as a function of temperatures.

Metal site	100 K	185 K	273 K
U1	0.6442 (1)	0.313 (0.5)	0.205 (0.5)
U2	0.1903 (1)	0.0192 (0.5)	0.0518 (0.5)
U3	0.1087 (1)	0.0630 (0.5)	0.0498 (0.5)
U4	0.0566 (1)	0.082 (0.5)	0.0427 (0.5)
U5		0.0315 (0.5)	0.0422 (0.5)
U6			0.0210 (0.5)
U7			0.0251 (0.5)
U8			0.0246 (0.5)
U9			0.0408 (0.5)
U10			0.0193 (0.5)
U11			0.01091 (0.5)

The occupancy rate of the carbon cage corresponding to the metal site is in the brackets.

Supplementary Table 5. Metal site occupancy in UN@C_2(5)-C_{82} as a function of temperatures.

Metal site	100 K	185 K	273 K
U1	0.312 (0.5)	0.289 (0.5)	0.260 (0.5)
U2	0.188 (0.5)	0.211 (0.5)	0.079 (0.5)
U3			0.055 (0.5)
U4			0.0265 (0.5)
U5			0.0303 (0.5)
U6			0.068 (0.5)
U7			0.0202 (0.5)

The occupancy rate of the carbon cage corresponding to the metal site is in the brackets.

Supplementary Table 6. Crystal data of UN@C_s(6)-C_{82}.

Crystal	**UN@C_s(6)-C_{82} at 100K**	**UN@C_s(6)-C_{82} at 185 K**	**UN@C_s(6)-C_{82} at 273 K**
Formula weight	1986.26	1986.82	1987.39
Crystal system	monoclinic	monoclinic	monoclinic
Space group	*C*2/*c*	*C*2/*m*	*C*2/*m*
***a*, Å**	25.3086(13)	25.3712(6)	25.4546(11)
***b*, Å**	14.9637(7)	15.0697(3)	15.2260(6)
***c*, Å**	39.809(2)	19.9969(5)	20.0570(9)
***α*, deg**	90	90	90
***β*, deg**	94.401(2)	94.6860(10)	95.1660(10)
***γ*, deg**	90	90	90
Volume, Å^3	15031.6(13)	7620.0(3)	7741.9(6)
Z	8	4	4
***T*, K**	100	185	273
Radiation (*λ*, Å)	Synchrotron Radiation (0.82641)	Synchrotron Radiation (0.82641)	Synchrotron Radiation (0.82641)
Unique data (R_{int})	14570 (0.0624)	7664 (0.0673)	7772 (0.0473)
Parameters	1288	1048	1111
Restraints	1082	1383	1516
Observed data ($I > 2\sigma(I)$)	13753	7127	7039
R_1 (observed data)	0.0764	0.0831	0.0995
wR_2 (all data)	0.1961	0.2342	0.2581
CCDC NO.	2120710	2120939	2120731

Supplementary Table 7. Crystal data of UN@C_2(5)-C_{82}.

Crystal	**UN@C_2(5)-C_{82} at 100K**	**UN@C_2(5)-C_{82} at 185K**	**UN@C_2(5)-C_{82} at 273K**
Formula weight	1987.44	1987.46	1987.69
Crystal system	monoclinic	monoclinic	monoclinic
Space group	*C*2/*m*	*C*2/*m*	*C*2/*m*
***a*, Å**	25.3001(8)	25.3680(6)	25.463(2)
***b*, Å**	14.9553(4)	15.0340(3)	15.1781(13)
***c*, Å**	19.9754(6)	20.0363(4)	20.1103(18)
***α*, deg**	90	90	90
***β*, deg**	94.7540(10)	94.8360(10)	95.028(3)
***γ*, deg**	90	90	90
Volume, Å^3	7532.1(4)	7614.3(3)	7742.4(12)
Z	4	4	4
***T*, K**	100	185	273
Radiation (*λ*, Å)	Synchrotron Radiation (0.82641)	Synchrotron Radiation (0.82641)	Synchrotron Radiation (0.82641)
Unique data (R_{int})	7510 (0.0566)	7600 (0.0488)	7757 (0.0479)
Parameters	1029	1029	1068
Restraints	1384	1376	1437
Observed data ($I > 2\sigma(I)$)	7055	7069	7013
R_1 (observed data)	0.1026	0.1065	0.1211
wR_2 (all data)	0.2400	0.2718	0.3054
CCDC NO.	2050571	2120708	2120709

Supplementary Table 8. Adiabatic spin-state relative energies (ΔE, kcal·mol^{-1}) and U Mulliken Spin Populations (MSP) for UN@C_2(5)-C_{82} and UN@C_s(6)-C_{82} using different functionals: PBE, BP86, PBE0 and B3LYP.

Isomer	Spin state	PBE	MSP	BP86	MSP	PBE0	MSP	B3LYP	MSP
C_2(5)-C_{82}	Doublet	5.3	0.8	4.3	0.9	2.9	1.2	2.4	1.2
	Quartet	23.2	1.0	21.8	1.1	23.5	1.2	22.7	1.2
C_s(6)-C_{82}	Doublet	0.0	0.5	0.0	0.7	0.0	1.2	0.0	1.2
	Quartet	16.6	0.9	15.8	1.0	17.1	1.2	16.1	1.2

Supplementary Table 9. Comparison of the calculated N-U distance (in Å) using different functionals: PBE, BP86, PBE0 and B3LYP, vs. the experimental value for UN@C_2(5)-C_{82} and UN@C_s(6)-C_{82}.

Isomer	Spin state	PBE	BP86	PBE0	B3LYP	Expt.
C_2(5)-C_{82}	Doublet	1.764	1.769	1.744	1.758	1.760
C_s(6)-C_{82}	Doublet	1.760	1.764	1.744	1.759	1.754

Supplementary Table 10. Adiabatic spin-state relative energies (ΔE, kcal·mol^{-1}) and U Mulliken Spin Populations (MSP) for UN@C_2(5)-C_{82} and UN@C_s(6)-C_{82} using different software: ADF vs. G16.

		ADF/PBE/TZP/D3		G16/PBE/6-31G** & SDD/D3	
	Spin state	ΔE	MSP (U)	ΔE	MSP (U)
C_2(5)-C_{82}	Doublet	5.3	0.8	5.5	0.8
	Quartet	23.2	1.0	23.5	1.0
C_s(6)-C_{82}	Doublet	0.0	2.0	0.0	0.5
	Quartet	16.6	2.6	16.4	0.9

Supplementary Table 11. Comparison of the calculated N-U distance (in Å) using ADF vs. G16. The data are compared to the corresponding experimental value for UN@C_2(5)-C_{82} and UN@C_s(6)-C_{82}.

Isomer	Spin state	ADF/PBE/TZP/D3	G16/PBE/6-31G**&SDD/D3	Expt.
C_2(5)-C_{82}	Doublet	1.764	1.755	1.760
C_s(6)-C_{82}	Doublet	1.760	1.750	1.754

Supplementary Table 12. Relative energies (in kcal·mol^{-1}) and structural parameters (distances in Å) of UN, obtained with ZORA/PBE/TZP/D3 for optimized UN@C_2(5)-C_{82} spin-doublet geometries with different orientation of the UN cluster inside the C_2-C_{82} cage.

Orientation	Erel	d(U-N)	d(U-C1 cage)	d(U-C2 cage)	d(U-C3 cage)	d(U-C4 cage)
U1	0.0	1.764	2.634	2.515	2.503	2.624
Ori1	1.7	1.758	2.506	2.514	2.516	2.534
Ori2	2.5	1.763	2.479	2.511	2.596	2.563

Supplementary Table 13. Relative energies (in kcal·mol^{-1}) and structural parameters (distances in Å) of UN, obtained with ZORA/PBE/TZP/D3 for optimized UN@C_s(6)-C_{82} spin-doublet geometries with different orientation of the UN cluster inside the C_s-C_{82} cage.

Orientation	Erel	d(U-N)	d(U-C1 cage)	d(U-C2 cage)	d(U-C3 cage)	d(U-C4 cage)
U1	0.0	1.760	2.476	2.506	2.551	2.631
Ori1	7.6	1.756	2.451	2.518	2.511	2.543
Ori2	4.4	1.753	2.517	2.523	2.545	2.563
Ori3	11.2	1.757	2.504	2.552	2.503	2.552

Supplementary Table 14. U-N distance in UN@C_s(6)-C_{82} as a function of temperatures.

Metal site	**100 K / Å**	**185 K / Å**	**273 K / Å**
U1-N1	1.760	1.740	1.774
U2-N1	1.681	1.750	1.717
U3-N1	1.733	1.801	1.683
U4-N1	1.820	1.736	1.756
U5-N1		1.724	1.721
U6-N1			1.750
U7-N1			1.720
U8-N1			1.744
U9-N1			1.714
U10-N1			1.730
U11-N1			1.670

xyz coordinates

Spin-doublet ground state geometry of UN@C_2(5)-C_{82}

C	-29.950820	-49.383223	51.204911
C	-31.336072	-49.491651	50.860173
C	-31.551608	-50.841936	50.362155
C	-30.287081	-51.521607	50.303358
C	-29.291849	-50.624094	50.836733
C	-28.016146	-50.589755	50.288222
C	-27.348254	-49.321455	50.087689
C	-27.960528	-48.138284	50.483575
C	-29.297951	-48.166688	51.048118
C	-30.012640	-47.016461	50.559680
C	-31.368909	-47.098320	50.137767
C	-32.044420	-48.381397	50.324928
C	-33.144966	-48.697820	49.466997
C	-33.416140	-50.038088	49.035405
C	-32.573826	-51.123572	49.422070
C	-32.336577	-52.155088	48.468984
C	-31.062483	-52.801791	48.390467
C	-29.978788	-52.420232	49.240082
C	-28.625193	-52.392673	48.670667
C	-27.683561	-51.453227	49.182997
C	-26.805691	-50.720704	48.314252
C	-26.653123	-49.374851	48.833599
C	-26.565679	-48.258672	47.970460
C	-27.163563	-46.995806	48.414042
C	-27.833552	-46.971564	49.664489
C	-29.058650	-46.214748	49.830641
C	-29.486417	-45.348366	48.856450
C	-30.884434	-45.260595	48.529839
C	-31.819774	-46.182083	49.079276
C	-32.940282	-46.561231	48.223930
C	-33.594151	-47.809126	48.449985
C	-34.204781	-48.586395	47.375105
C	-34.034925	-49.979932	47.739961
C	-33.727816	-50.981538	46.755854
C	-32.888701	-52.057569	47.133224
C	-31.924378	-52.635038	46.214250
C	-30.840379	-53.138136	47.005267
C	-29.560267	-53.132454	46.472515
C	-28.436824	-52.769056	47.312244
C	-27.478587	-52.110207	46.476974
C	-26.731926	-50.984763	46.932079
C	-26.428534	-49.883812	46.022442
C	-26.359790	-48.516367	46.544644
C	-26.584435	-47.447685	45.645717
C	-27.245206	-46.229020	46.068131
C	-27.572168	-46.005579	47.420171
C	-28.705810	-45.176038	47.659025
C	-29.607581	-44.812260	46.603227
C	-30.942013	-44.835666	47.157199
C	-32.006119	-45.220463	46.351220
C	-33.033331	-46.056711	46.893239
C	-33.569154	-46.862723	45.802682
C	-34.208526	-48.129818	46.006846
C	-33.952833	-49.153248	44.990076
C	-33.665368	-50.531739	45.387080
C	-32.618504	-51.044100	44.536896
C	-31.695281	-52.070356	44.932597
C	-30.353433	-52.048393	44.362073
C	-29.327749	-52.661001	45.134910
C	-27.987135	-52.136864	45.128028
C	-27.628072	-51.152619	44.245441
C	-26.756243	-50.066736	44.652885
C	-27.047240	-48.965754	43.789413
C	-26.930820	-47.665559	44.269459
C	-27.883677	-46.650985	43.876235
C	-28.085502	-45.768551	44.995506
C	-29.357294	-45.177424	45.250845
C	-30.487572	-45.545503	44.389776
C	-31.795829	-45.553697	44.968074
C	-32.766064	-46.552024	44.627176
C	-32.464513	-47.560193	43.667885
C	-33.038614	-48.859533	43.891309
C	-32.244239	-50.022899	43.614914
C	-30.934938	-49.968823	43.026159
C	-29.970935	-50.999462	43.403829
C	-28.594860	-50.649655	43.295594
C	-28.170190	-49.323424	42.939094
C	-29.102848	-48.352595	42.586551
C	-28.952442	-46.984369	43.045303
C	-30.262721	-46.451307	43.312038
C	-31.219443	-47.484414	42.999069

C	-30.495186	-48.685291	42.609897
N	-30.146979	-48.776739	46.812675
U	-31.826818	-48.889506	46.284780

Spin-doublet ground state geometry of UN@C_s(6)-C_{82}

U	15.942839	8.772680	14.376455
N	16.551046	7.290517	13.648367
C	15.319412	10.932507	15.414580
C	16.589338	10.688103	16.059756
C	16.792286	9.646909	17.062362
C	15.757382	8.716571	17.395698
C	14.511488	8.901085	16.712670
C	14.262031	9.998130	15.774566
C	13.357060	9.447603	14.765775
C	13.419307	9.814134	13.381553
C	14.487838	10.691245	13.016680
C	15.417689	11.240510	13.999102
C	16.707306	11.318518	13.316180
C	17.957206	11.151821	13.988959
C	17.873607	10.843888	15.384153
C	18.820009	9.960005	15.978785
C	18.151696	9.217826	17.012944
C	18.532338	7.871004	17.331277
C	17.506753	6.979502	17.754668
C	16.120447	7.402485	17.773814
C	15.299175	6.265353	17.415419
C	14.150695	6.404386	16.589952
C	13.766143	7.750480	16.292666
C	13.056817	8.085216	15.101721
C	12.671213	7.093255	14.143220
C	12.509670	7.559440	12.809719
C	12.969245	8.880622	12.421416
C	13.601739	8.772637	11.120479
C	14.808207	9.470074	10.831878
C	15.191521	10.461878	11.788055
C	16.553407	10.849647	11.972608
C	17.616133	10.255030	11.225194
C	18.887403	10.249730	11.863291
C	19.048872	10.651815	13.243196
C	20.025674	9.773945	13.859278
C	19.895364	9.384574	15.221685
C	20.315816	8.075003	15.576598
C	19.636542	7.320653	16.628389
C	19.668339	5.936092	16.280123
C	18.580534	5.060990	16.579887
C	17.548877	5.589246	17.408132
C	16.181951	5.145699	17.261058
C	15.856396	4.151582	16.355827
C	14.633454	4.218972	15.602564
C	13.796470	5.368119	15.628761
C	13.045492	5.707707	14.409473
C	13.177076	4.855034	13.276254
C	13.059922	5.355177	11.932259
C	12.723861	6.684371	11.695539
C	13.398122	7.432742	10.653286
C	14.384204	6.826058	9.882756
C	15.590354	7.534431	9.542365
C	15.864261	8.838300	10.045619
C	17.269377	9.224439	10.253630
C	18.277494	8.265301	9.963325
C	19.509289	8.206198	10.705177
C	19.821287	9.186294	11.628965
C	20.483148	8.846187	12.868008
C	20.768610	7.489341	13.194490
C	20.764667	7.154203	14.582800
C	20.390004	5.830905	15.031590
C	20.053433	4.855761	14.113720
C	18.977174	3.934638	14.394334
C	18.233673	4.017213	15.607537
C	16.892531	3.556017	15.534365
C	16.289077	3.186292	14.288027
C	14.886368	3.511697	14.375016
C	14.179695	3.817606	13.241209
C	14.830090	3.820234	11.943519
C	14.075711	4.714341	11.115870
C	14.722507	5.432920	10.115293
C	16.133426	5.268062	9.927103
C	16.633093	6.542564	9.444143
C	17.939740	6.902367	9.650496
C	18.833735	6.012663	10.350743
C	19.833291	6.820938	10.985080
C	20.422595	6.446568	12.221743
C	20.072436	5.150147	12.700307
C	19.027738	4.381314	12.100138

C	18.351896	3.631171	13.145482
C	16.977885	3.317954	13.046111
C	16.240115	3.698767	11.836588
C	16.920749	4.454948	10.783568
C	18.331314	4.821136	10.952220